Cyclically symmetric radially self-similar phononic pseudocrystal isolator for broadband, ultrasonic vibration bandstop filtering

S. H. Swift,[1, a)] Ihab F. El-Kady,[1] Rick A. Kellogg,[2] Dale E. Cillessen,[2] and Michael Denison[2]
[1)] *Photonic and Phononic Microsystems Department, Sandia National Laboratories, Albuquerque, NM 87123 USA.*
[2)] *Sandia National Laboratories, Albuquerque, NM 87123 USA*

(Dated: 12 February 2025)

A 2-D phononic pseudocrystal isolator exhibiting cyclic symmetry and radial self-similarity is measured and demonstrated to block a wide range of ultrasonic vibration. Measurements of longitudinal and shear wave blocking effects are made and compared with computational results. The use of the bandgap edge ratio is recommended for quantifying suppression in very-wide-bandgap materials. The upper-to-lower suppression edge frequency ratios of 3–4 are remarkably large for shear waves, and even larger for longitudinal waves upper-to-lower suppression ratio (13 at 5 dB), such that 92.5% of frequencies in that range experience ≥5 dB of suppression.

PACS numbers: 63.22.-m; 63.20.dk; 43.35.+d, 43.20.Tb

Phononic crystals are by now well-known for their ability to produce bandgaps blocking transmission of finite frequency ranges of sound in fluids or vibration in solids[1]. However, typical phononic crystals tend to exhibit modest bandgaps; for example, a study of wave guiding describes a typical square unit cell with a circular hole exhibiting a bandgap from 149 kHz to 202 kHz giving an upper-to-lower bandgap edge ratio of 1.356 (bandgap-to-midgap ratio of 0.302)[2]. A mechanical crosstalk reduction application employed bandgaps from 2.1–2.13 MHz and from 2.07–2.17 MHz (bandgap edge ratios of 1.014 and 1.048, respectively)[3]. Some exotic structures exhibit quite large bandgaps, e.g., with an edge ratio of 2.086[4]; however, these structures involve long thin spider-like structures, and appear unsuitable for structural applications.

Recent developments—often described using terms such as "rainbow trapping"[5] or "chirped phononic crystals"[5,6]—suggest it may be possible to block an enlarged range of frequencies using phononic structures by employing changing unit cell sizes. For example, Ref. 5 demonstrates this principle by gradually changing the local unit cell feature size in a grooved plate, expanding a bandgap with an upper-to-lower band edge ratio of about 1.35 to about 1.87. Similar expansion of the range of frequencies blocked has been demonstrated acoustically with an array of cylinders of variable spacing[6].

Tapered two-dimensional examples of this broadband isolation mechanism have recently been proposed by a number of researchers beginning with computational studies of phononic pseudocrystals exhibiting cyclic symmetry and radial self-similarity[7–9], and quickly coming to include both measured and computational results for the out-of-plane motion of lattice truss structures (laid out using similar principles[10–12]), and the out-of-plane motion of more ordinary phononic pseudocrystals[13]. Part of this effort has been spurred by the emerging need to provide vibration isolation in the MHz range[3,14] (e.g., between ultrasonic power and data channels in order to prevent mechanical crosstalk). However, the usefulness of structures that provide lower-frequency broadband vibration suppression while maintaining structural integrity cannot be overstated: such could isolate inertial measurement units from above-Nyquist vibration that would otherwise be aliased as noise, protect sensitive quantum sensors from noxious vibration, or serve as part of the vibration mitigation for future gravity-wave-detection instruments.

Nevertheless, this paper will focus on a fundamental demonstration of a 3D-printed cyclically symmetric and radially self-similar phononic pseudocrystal isolators providing broadband isolation at ultrasonic frequencies less than 10 MHz. This paper describes the use of laser powder bed fusion (or additive manufacturing generally) to construct a 2D phononic pseudocrystal isolator. Although shear wave suppression has been measured previously, we additionally show longitudinal insertion loss measurements of phononic pseudocrystal patterning for 2D phononic pseudocrystal isolators. We will also show shear wave suppression properties using a finite element model for comparison. These structures block a large frequency band, effectively, a band stop-type behavior.

Our phononic pseudocrystal was designed with 120 circumferential holes per row, resulting in a radial self-similarity ratio of ∼1.05. The largest hole has a nominal diameter of 0.004 m (making the nominal maximum unit cell length 0.0046 m), while the smallest hole has a nominal diameter of 0.00046 m as shown in Fig. 1. The pseudocrystal upper surface is conical for the first 24 holes, descending from planar at an angle of 3.4^o. The inner region is also conical, but sloped in the opposite direction at 26.3^o from planar. The transition is smoothed by a fillet with radius of 2 cm. The reversal of slope and consequent deviation from self-similar behavior near the central region was designed to allow sufficient thickness

[a)] Electronic mail: shswift@sandia.gov.

for the mounting of transducers on the interior surface without overhang. The first 24 stations are unaffected by the inclusion of the fillet, and are designed with precisely self-similar structure, and we limit our shear wave investigation to this region where the self-similarity condition fully holds. Conceptually, our unit pseudocell is modeled on the structure of Ref. 2, with a square local unit cell with a circular hole in the center; however, to increase structural integrity, we altered the parameters to include a radius-to-cell side-length ratio of 0.43 and a thickness-to-cell length ratio of 1.321. The band structure of the unit cell associated with the exterior conical region reveals that *the "local" unit cell does not exhibit a total bandgap* in the first 360 eigenvalues (for the largest hole, covering 0–2.46 MHz), or when considering only the radial direction of propagation (see additional figures and discussion in the supplemental material). All smaller holes within the self-similar region have a scaled version of this same local dispersion relation and, consequently, the phenomena exhibited in this paper cannot be ascribed to total *local* bandgaps, even under the restriction of radial propagation. However, given that (1) a wave cannot change frequency, (2) the local modal surface on which a wave is traveling tends to change frequency with scale, (3) many modal surfaces have a have a minimum local bounding frequency (even without a bandgap), and (4) the size of a local unit pseudocell can be reduced until the lower bound of the local manifestation of the mode (within which an elastic wave is propagating) exceeds the frequency of a given wave: our structure can exhibit a substantial effective *global* bandgap even in the absence of a *local* bandgap[8,10,11].

Phononic pseudocrystal isolators were fabricated from stainless steel 316L using laser powder-bed fusion with a 15-45 μm particle size in a Renishaw AM400, which utilizes a 1064-nm laser with 0.07-mm average spot size. The pseudocrystal was prepared for manufacturing using Renishaw's QuantAM software. During the slicing process, the following settings were applied: 200-W laser power, 0.75-m/s laser velocity, 0.11-mm hatch spacing, and 0.05-mm layer thickness.

Some deviations from the designed geometry were observed after manufacturing; specifically, hole diameters were consistently 0.25 mm smaller[13]. This hole diameter reduction occurred because the powder-interactive spot size was larger than the laser-theoretical spot size based on the selected process settings. Interactive spot size optimization for this design was not performed prior to manufacturing the phononic pseudocrystal. Additionally, the tapered surfaces exhibited increased surface roughness, likely due to the deposition of layers of metal with fixed thickness and the selected particle size. In contrast, the non-tapered surface, which was finished using wire electrical discharge machining (EDM), exhibited a significantly smoother finish.

Finite element method calculations were performed using COMSOL's Solid Mechanics interface. The material parameters used to model steel as a linear elastic material are given in Table I. Longitudinal and vertically polarized shear waves were modeled using the half-channel boundary conditions of Ref. 15 (symmetry in this case) to reduce the domain size. A boundary load was applied at the channel exterior boundary (left end of inset in Fig. 4), and a Low-Reflecting Boundary condition was applied at the interior boundary (right end of inset in Fig. 4). A free triangular mesh was employed with a maximum element size of 0.3 mm, providing a rough grid of $3.\bar{4}$ free triangular mesh elements per shear wavelength at 3 MHz and more at lower frequencies (and for longitudinal waves); however, most shear behavior of interest takes place at $f \leq 1.5$ MHz, providing $6.\bar{8}$ or more elements per wavelength available to us. The total number of elements was 309,025.

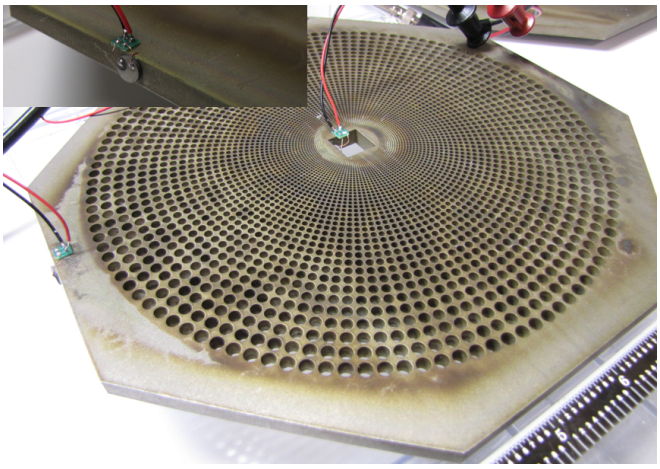

FIG. 1. The patterned plate is shown with printed circuit boards (PCB) and longitudinal tranducers. (inset) The unpatterned plate with piezoelectric transducer and PCB.

ρ	7,900 kg/m^3
c_p	5,790 m/s
c_s	3,100 m/s

TABLE I. Linear elastic material parameters for steel material model.

For the longitudinal wave measurement, cyanoacrylate was used to affix Boston Piezo-Optics Inc. PZT-4 piezoelectric tiles with a 0.25-in diameter, 1.15-mm thickness, and a nominal 2-MHz resonance frequency to the interior cutout region of the patterned and unpatterned plates plates, and to the nearest exterior boundary along a line of holes as shown in Fig. 1. These were excited using an NI PXI-5412 single-channel output in connection with a pair of NI PXI-6653 timing modules, and an NI PXI-5105 card acquired the signals; the computer controller was an NI PXI-5412. A Mini Circuits ZHL-3A Class-A amplifier with maximum output of 24 Volts was used for output amplification, and an Olympus 5682 preamplifier with fixed 30-dB gain amplified the measured signal. To isolate the effects of the pseudocrystal hole pattern on vibra-

tion transmission, the measurement was repeated both with a patterned plate, and an unpatterned plate tapered in the same way and made using the same manufacturing process keeping other aspects of the measurement chain the same. The ratio of the transmission allowed by the two plates thus allows us to calculate an insertion loss for the hole pattern itself, isolating this measure from potential confounding factors such as transducer response or effects originating from the tapered plate thickness. The plate was supported on the edges perpendicular to the line containing the two transducers to avoid providing either alternative propagation paths or additional damping.

The plate was excited by a chirp signal from 0.1–10 MHz; the signal-to-noise ratio was at least 15 dB for frequencies between 0.14–10.00 MHz. To include electromagnetic transmission in the noise figure and ensure that vibratory transmission predominated, the signal-to-noise ratio was assessed with the drive system active, but unattached. The power spectral density was calculated using MATLAB's Welch's method implementation with 8,192-point (1.3653×10^{-4} sec) discrete Fourier transforms, Hann windows of the same length, and 50% overlap. This process was repeated for nine time records each of length 0.040 seconds, sampled at 60 MHz for 2.4×10^6 samples per record. The mean and standard deviation were calculated across the ensemble of nine records for both the patterned and the unpatterned plate measurements. These standard deviations were then combined using the rule $\sigma_{total} = \sqrt{\sigma_p^2 + \sigma_u^2}$ (σ_p and σ_u are the standard deviations for the patterned and unpatterned ensemble measurements), and σ_{total} is shown as a shaded region surrounding the transmission loss in Fig. 2; however, this region is not easily visible because very little variation in the transmission properties occurred across measurement runs.

The pseudocrystal patterning resulted in substantial additional vibration isolation between 0–3 MHz as shown in Fig. 2. From 0.227–2.864 MHz the suppression is typically between 5–25 dB, with occasional excursions outside of that range. Uninterrupted suppression of $\geq$5 dB is present from 1.296–1.685 MHz and from 1.707–2.864 MHz, and between 0–3 MHz, 89% of the frequency bins had suppression of $\geq$5 dB, as did 92.5% of frequencies between 0.227–3 MHz: an effective suppression edge ratio of 13.2, albeit with some intermittency. Although no complete bandgap is present in the *local* dispersion in the range of frequencies considered in the outer patterned region, a remarkably large band of frequencies was effectively blocked. The feature at around 6 MHz is due to a slight difference in the resonance frequency between the transducers on the patterned and unpatterned plates, and is unrelated to insertion loss. Computational results suggest the potential for continuous 20-dB suppression of longitudinal waves between $\sim$.2 MHz and 3^+ MHz; however, manufacturing geometric tolerances (discussed more in connection with the SLDV results) likely inhibited the real built structure from closely approximating the idealized results.

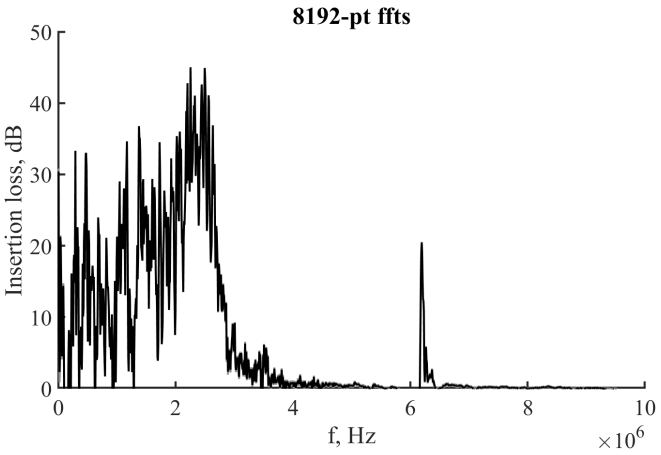

FIG. 2. Radially-oriented longitudinal wave insertion loss (with gray shaded standard deviation) associated with the hole pattern vs a plate with similar geometry but no phononic pseudocrystal patterning.

For the SLDV measurement, a STEMINC SMPL60W05T21F27R transducer with dimensions $60 \times 5 \times 2.1$ mm and a 27 kHz nominal resonance frequency was affixed to the flat face of each barrier using 3M Scotch-Weld DP460 epoxy cured under vacuum to guard against voiding. SLDV measurements were performed using a Polytec PSB-500-HV in high-frequency sampling mode, measuring at 25 MHz. The Mini Circuits ZHL-3A Class A drive-side amplifier used in the other experiment was used here. Retroreflective tape enhanced the return signal from the laser (Fig. 3, with an inset showing the scanning stations). Supports at the corners were employed to avoid spurious damping and the creation of mechanical conduction paths around the pseudocrystal region. The first 24 scan points were in the outer self-similar region, and these will be the focus of the analysis; their locations were chosen to align with the webbing of the structure. For ease of comparison, the computational results are expressed using station locations similar to the measured positions. The initial extraction of data from COMSOL was performed using a Line Graph with a Cut Line running adjacent to the flat side of the outer edge, as shown in Fig. 4 (inset).

Excitation consisted of a burst chirp signal from 0.8–5 MHz. However, spectral analysis of the received signals suggests that substantial spectral content (down to $\sim$0.27 MHz) was excited at the outermost station. To account for frequency-dependent excitation imparted by the transducer, the measured and calculated vertically polarized shear displacement values are normalized by the peak value at each frequency across all stations. Additional spectral smoothing was performed for the measured result using a 10-pt moving average. The same suppression pattern is visible in both the SLDV-measured results and the computational predictions: as the station position increases, a suppression region of in-

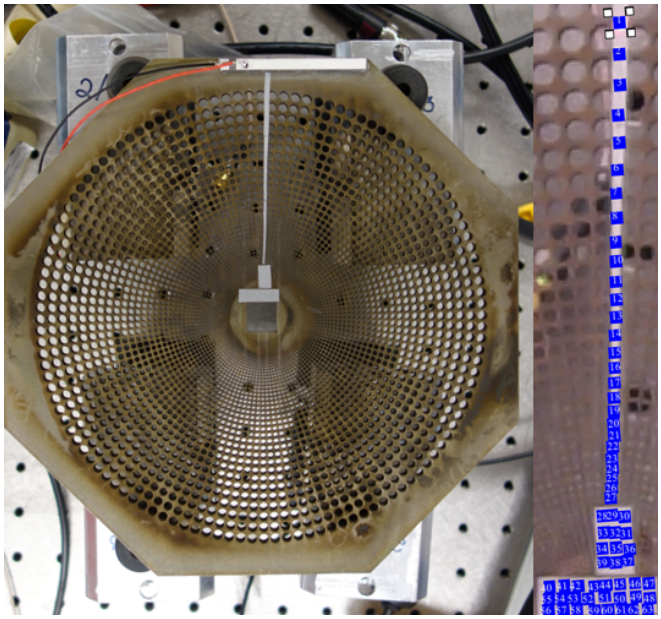

FIG. 3. Pseudocrystal with piezoelectric transducer affixed. (inset) Scanning stations.

creasing frequency range opens. Although the lack of a bandgap results in no suppression at the station closest to the excitation point, as the local pseudocell size changes, the local dispersion relation is scaled, and an increasing range of frequencies are suppressed. In the measured result, a line of peaked values is apparent just before the (nearly triangular in frequency and station) suppression region. These peaked values result from constructive interference between forward- and backward-traveling waves near where the propagating mode becomes unavailable. Tian *et al* observed a similar effect in which energy in a graded phononic crystal accumulated shortly before the position where the group velocity reached zero.[16] In both the measured and the computationally predicted results, the suppressed frequency range is between ∼0.3 or 0.4 MHz and about 1.25 MHz, an upper-to-lower suppression edge ratio of ∼4.2 or 3.1 for the computational or measured results, respectively, which can also be expressed as a bandgap-to-midgap ratio of 1.225 or 1.03. This ratio is much larger than the typical bandgap-to-midgap ratio of the conventional phononic crystal in Ref. 2, which served as the loose model our unit pseudocell. In some respects, the larger suppression ranges enabled by ideal phononic pseudocrystals present a problem when expressed in terms of the bandgap-to-midgap ratio $r_{BG/MG}$:

$$r_{BG/MG} = 2\frac{f_{upper} - f_{lower}}{f_{upper} + f_{lower}}; \tag{1}$$

because this measure has a theoretical limit of 200% and, thus, an upper asymptote of two (corresponding to a case in which the upper bound of the suppression range f_{upper} *does not exist* and the lower bound f_{lower} is finite),

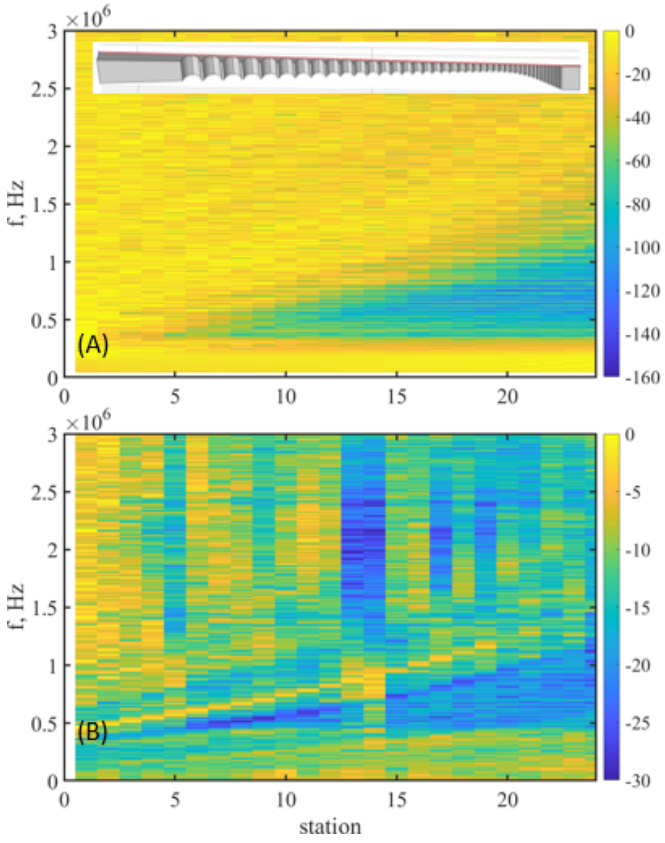

FIG. 4. Levels of vertical vibration normalized by the maximum at each frequency in simulation (A) and SLDV measurement (B). Model shown in inset of (A).

the measure becomes decreasingly descriptive with larger bandgaps. Consequently, we recommend the upper-to-lower suppression edge ratio

$$r_{U/L} = \frac{f_{upper}}{f_{lower}} \tag{2}$$

as this both contains the same information and, by expressing it in an easier-to-visualize manner, remains relevant for truly broadband suppressors.

Some notable differences exist between the measured and calculated results, and these deserve attention. The calculated result was able to ensure radial incidence of the elastic waves, a condition more difficult to obtain in an experiment where waves approach the structure at a variety of angles of incidence. Additionally, surface roughness and slight shrinkage of holes due to the manufacturing process lead to small-scale geometric differences between the artifact and its computational model; unsurprisingly, hole size irregularities tend to degrade performance, both in suppression range and suppression depth[13]. We anticipate that greater similarity between model and test artifact will result in greater concordance of results.

Furthermore, it is likely that the combination of geometric uncertainty and employing a design that involved

neither a total bandgap nor a directional bandgap may have increased the degree of performance decrement associated with geometric uncertainty. Total bandgaps provide a buffer region in which no wave can travel, likely reducing the opportunities for trapped modes to project onto compatible modes via tunneling. As a result, designs based on such bandgaps are likely to exhibit less sensitivity to geometric tolerancing.

Broadband longitudinal and vertically polarized shear wave suppression were demonstrated in measurements of a phononic pseudocrystal with a pseudocell built on the model of a unit cell that does not contain any total bandgaps in the relevant frequency range, or any radial-direction bandgaps. These measurements and the associated artifact constitute a demonstration of broadband vibration isolation by a non-truss-based 2D phononic pseudocrystal, including a longitudinal wave measurement of a phononic pseudocrystal. As such, they confirm that mechanical band-stop filtering over a wide frequency range is possible in a mechanically robust structure. Upper-to-lower suppression edge frequency ratios of 3.1–4.2 (bandgap-to-midgap ratios of 1.03–1.2) were observed for shear waves, and on the order of 13.2 (bandgap-to-midgap ratio of 1.7) for longitudinal wave insertion loss, depending on the criteria employed. However, we note that the large suppression ranges realized may necessitate a change in the figures of merit used to assess phononic vibration suppression structures because the bandgap-to-mid-gap ratio becomes insensitive for comparisons between large suppression ranges; for this purpose we recommend the bandgap or suppression edge ratio.

SUPPLEMENTARY MATERIAL

See the supplementary material for information connecting the bandgap observed during the SLDV scans with the dispersion relations along the First Brillouin Zone, and the mode structure and polarization of the waves supported by the local unit cell. Additionally, the supplementary materials contains animations of the vertically-polarized shear mode that appears to be dominant at the point of extinction in the SLDV analysis and the pseudocrystal simulation as well as an animation of the pseudocrystal simulation to compare the motion of the pseudocrystal to the identified mode as it approaches extinction.

Sandia National Laboratories is a multi-mission laboratory managed and operated by National Technology Engineering Solutions of Sandia, LLC (NTESS), a wholly owned subsidiary of Honeywell International Inc., for the U.S. Department of Energy's National Nuclear Security Administration (DOE/NNSA) under contract DE-NA0003525. This written work is authored by an employee of NTESS. The employee, not NTESS, owns the right, title and interest in and to the written work and is responsible for its contents. Any subjective views or opinions that might be expressed in the written work do not necessarily represent the views of the U.S. Government. The publisher acknowledges that the U.S. Government retains a non-exclusive, paid-up, irrevocable, world-wide license to publish or reproduce the published form of this written work or allow others to do so, for U.S. Government purposes. The DOE will provide public access to results of federally sponsored research in accordance with the DOE Public Access Plan.

[1] M. I. Hussein, M. J. Leamy, and M. Ruzzene, Sci. Rep. **7**, 40004 (2014).
[2] M. G. Baboly, A. Raza, J. Brady, C. M. Reinke, Z. C. Leseman, and I. F. El-Kady, Appl. Phys. Lett. **109**, 183504 (2016).
[3] C. Sugino, R. Gerbe, E. Baca, C. Reinke, M. Ruzzene, A. Erturk, and I. El-Kady, App. Phys. Lett. **120**, 191705 (2022).
[4] H. Xiang, X. Ma, and J. Xiang, Materials **13**, 2106 (2020).
[5] Z. Tian and L. Yu, Sci. Rep. **7**, 40004 (2017).
[6] R. P. V. Romero-García, A. Cebrecos, V. J. Sánchez-Morcillo, and K. Staliunas, Appl. Phys. Lett. **102**, 091906 (2013).
[7] S. H. Swift, C. B. Smith, R. A. Kellogg, and I. F. El-Kady, J. Acoust. Soc. Am. **153**, A317 (2023).
[8] S. H. Swift, I. F. El-Kady, and R. A. Kellogg, "Principles underlying 2-d phononic pseudocrystal isolators," in 6^{th} *International Conference on Phononic Crystals/Metamaterials/Metasurfaces, Phonon Transport, and Topological Phononics* (International Phononics Society, Albuquerque, 2023) pp. 344–345, PHONONICS–2023–0212.
[9] S. H. Swift, J. Acoust. Soc. Am. **155**, A192 (2024).
[10] C. Dorn and D. M. Kochmann, "Conformally graded metamaterials for wave attenuation," in 6^{th} *International Conference on Phononic Crystals/Metamaterials/Metasurfaces, Phonon Transport, and Topological Phononics* (International Phononics Society, Albuquerque, 2023) pp. 164–165, PHONONICS–2023–0039.
[11] C. Dorn and D. M. Kochmann, Extreme Mech. Lett. **65**, 102091 (2023).
[12] B. Telgen, V. Kannan, J.-C. Bail, C. Dorn, H. Niese, and D. M. Kochmann, J. Mech. Phys. Solids **191**, 105762 (2024).
[13] S. H. Swift, M. H. Denison, and D. E. Cillessen, J. Acoust. Soc. Am. **155**, A32 (2024).
[14] C. Sugino, S. Oxendale, A. Allam, C. Arrington, C. S. John, E. Baca, J. Steinfeldt, S. H. Swift, C. Reinke, and I. El-Kady, "Experimental validation of crosstalk minimization in metallic barriers with simultaneous ultrasonic power and data transfer," in *2021 IEEE International Ultrasonics Symposium (IUS)* (IEEE, New Jersey, 2021) pp. 1–3.
[15] S. H. Swift, C. B. Smith, R. A. Kellogg, and I. F. El-Kady, Proc. Meet. Acoust. **51**, 022007 (2024).
[16] Z. Tian, C. Shen, J. Li, E. Reit, H. Bachman, J. E. S. Socolar, S. A. Cummer, and T. J. Huang, Nat. Com. **11**, 762 (2020).